Variable-Temperature Broadband Noise Characterization of MOSFETs for Cryogenic Electronics: From Room Temperature down to 3 K

Kenji Ohmori[1] and Shuhei Amakawa[2]

[1] Device Lab Inc., Tsukuba, Ibaraki, Japan, [2] Hiroshima University, Higashihiroshima, Hiroshima, Japan

Abstract

A broadband noise measurement system is newly developed and demonstrated at temperatures between 3 K and 300 K. Using the system, wideband noise spectroscopy (WBNS) from 20 kHz to 500 MHz is carried out for the first time, revealing that shot noise is the dominant white noise down to 3 K. The paper also suggests, by means of WBNS, the possibility of extracting the baseline noise characteristics, which do not include the noise component that varies a great deal from device to device.

(Keywords: cryogenic electronics, MOSFET, noise)

I. Introduction

Cryogenic and cold electronics are of intense interest for its potential use for quantum computing and high-performance computing [1,2]. At present, peripheral RF circuits for controlling the quantum processor operating in a millikelvin (mK) chamber lie outside the cryogenic chamber and are connected via many long RF cables. However, in a practically useful quantum computers, the number of qubits is expected to be more than a million. A promising approach is to locate the RF circuits in a 4 K chamber that encloses the mK chamber. Technically, this requires us to develop cryogenic RF circuits, where device noise models will be essential.

We reported broadband *in-situ* noise characterization of MOSFETs in temperature range from T = 300 K to 120 K at EDTM 2021 [3]. The lowest temperature of 120 K was dictated by the carrier freeze-out in bipolar transistors used in the low-noise amplifier (LNA). In this paper, we demonstrate a cryogenic noise measurement system capable of going down to 3 K.

II. Noise Measurement System Development

Fig. 1 shows (a) the cryogenic part and (b) a schematic of the noise measurement system developed. The system consists of a main board with a cryo-LNA and a replaceable device-under-test (DUT) board with three pins for connection. A DUT from a semiconductor foundry is mounted on it by flip-chip bonding. We characterized MOSFETs with gate lengths (L_g) of 120 and 180 nm, exhibiting similar tendencies. Results from the MOSFET with L_g = 180 nm will be presented in this paper. The system configuration is similar to that in [3,4], except that an external auxiliary amplifier is used for reducing the power consumption of the main board.

In order to compose the cryo-LNA, we screened various passive and active components for temperature stability between 300 K and 3 K. Microwave techniques were applied to design and characterize the cryo-LNA.

A Si diode located close (~1 cm) to the DUT board was used to sense the ambient temperature. The gain of the cryo-LNA is shown in **Fig. 2(a)**, demonstrating fairly stable characteristics over the target temperature (3–300 K) and frequency (20 kHz–500 MHz) ranges. The input-referred voltage noise of the cryo-LNA plus the auxiliary amplifier improves as the temperature is lowered (**Fig. 2(b)**), but it gradually bottoms out below 30 K due to the power consumption of the LNA (65 mW) at an ambient temperature of 4 K (near the DUT). Temperature of the LNA seems to remain higher in the cryogenic environment.

Extensive characterization of the system components was performed for precise DUT noise measurements, including cables, connectors, parasitics on the main and the DUT boards. Once the calibration is complete by going through several cooling cycles, the DUT noise can be measured in a single cooling cycle.

III. DC Characteristics of MOSFETs

Fig. 3 shows (a) I_d-V_g and (b) subthreshold swing (SS) of a MOSFET with L_g = 180 nm and a gate width of W_g = 10 µm. At temperatures below 50 K, SS bottoms out due to the band tail at the Si/SiO_2 interface [5].

In this paper, we mainly focus on the linear region of MOSFETs, in which both $1/f$ (flicker) noise and white noise are observable, and, in addition, the effect of self-heating is not significant [6]. V_g of 0.8 V was chosen, corresponding to strong inversion, where, as the temperature decreases, I_d increases as shown **Fig. 3**, due to the higher drift mobility for electrons.

IV. MOSFET Noise Characterization

A. Pure Thermal Noise

As was reported experimentally in [4], MOSFETs ideally generate only thermal noise under a zero drain bias (V_d = 0 V). **Fig. 4(a)** shows the drain current noise spectral density, S_{Id}, as a function of frequency f, exhibiting white noise that decreases as T decreases. The averaged S_{Id} from 200 kHz to 50 MHz are shown in **Fig. 4(b)** versus T together with the theoretical thermal noise intensity $4k_BT/R_{DUT}$, where R_{DUT} is the DUT resistance at V_d = 0 V. The results demonstrate that the new system has been precisely calibrated over the wide temperature range.

B. Transition from 1/f Noise to White Noise

Fig. 5(a) shows S_{Id} at V_g = 0.8 V with V_d ranging from 0 to 0.2 V at 300 K, demonstrating that the predominant noise clearly changes from $1/f$ noise to white noise as f becomes higher. S_{Id} at 5 K (**Fig. 5**(b)) behaves similarly, except that S_{Id} in the low-frequency (LF) region is larger than at 300 K, and that white noise depends greatly on V_d. Random telegraph noise (RTN) is observed at $V_d = 0.2\,V$ in **Fig. 5**(b), as a bump around 1 MHz. Since RTN results from a stochastic process involving carrier traps, it presents a major challenge for predictive noise modeling [7]. Under the measurement condition of the linear region, S_{Id} above 100 MHz is flat and can be treated as measured white noise S_w if RTN does not appear there (> 100 MHz).

C. Wideband Noise Spectroscopy –MOSFET Fingerprinting–

We carried out *wideband* noise spectroscopy (WBNS), which conventionally is carried out at lower frequencies and is referred to as low-frequency noise spectroscopy (LFNS) [8]. Our cryo-LNA approach enabled us to extend this methodology to the high-frequency (HF) white noise region for the first time.

Fig. 6 shows WBNS for V_g = 0.8 V with V_d = 0.1 V. Several sets of temperature-dependent peaks, originating from RTN, are clearly observed as fingerprints of individual traps in the MOSFET. Such data are often used to estimate the activation energy of carrier traps [8]. As T increases, an S_{Id} peak shifts to higher f because the trapping/detrapping probability increases. Note that a set of S_{Id} peaks associated with particular RTN appear only in a limited temperature range for a given f. This allows us to find a temperature range in which the effect of RTN disappears. By taking advantage of this, baselines (brown dot-dashed) for S_w (at f = 200 MHz) are drawn in **Fig. 6**. Similar approach can also be applied to the LF region, in which case the vertical axis should be S_{Idn} instead as it is more suitable for extraction of $1/f$ noise baselines.

D. White Noise Evaluation

Fig. 7 shows measured S_{Id} at 100 MHz, which can be regarded as white noise S_w (if RTN does not appear), as a function of V_d at three different temperatures (T = 300, 100, and 5 K). As can be seen from **Fig. 6**, RTN is less influential at 100 MHz for these temperatures. Also plotted in **Fig. 7** are thermal noise S_{th} (green), full-shot noise $2qI_d$ (orange), and the sum of these (blue). S_{th} intersects $2qI_d$ at $V_{d,cross} = 2k_BT/q$ [4], indicating that thermal noise dominates under low V_d ($< 2k_BT/q$) and shot noise becomes dominant otherwise. The values of $V_{d,cross}$ at T = 300, 100, and 5 K are 52, 17, and 0.8 mV, respectively. The intersections from measurement are denoted by the red arrows in **Fig. 7**. Note that as T decreases, shot noise dominates regardless of the value of V_d because $V_{d,cross}$ approaches 0 V. In addition, S_w for high V_d does not decrease because $S_{th}@300\ \mathrm{K} < 2qI_d@5\ \mathrm{K}$ under the strong inversion.

E. Fano Factor

The shot noise originates primarily from carriers crossing the potential barrier near the source [9]. Fano factor (or shot noise suppression factor) F is the ratio of S_w to full shot noise and satisfies $0 < F < 1$. F is calculated from a formula suitable for measurement-based evaluation [10]: $F = S_w/(2qI_d + S_{th})$. As V_g and V_d increase, F decreases owing to barrier lowering at the source [9]. We found in the T range from 300 to 120 K [4], that F gradually decreased as T decreased.

By using S_{Id} at 100 MHz shown in **Fig. 7**, F values at 300, 100, and 4 K were evaluated for V_g = 0.8 V with V_d = 0.1 V, and are 0.44, 0.36, and 0.29, respectively. The decrease in F down to 4 K were observed, being consistent with the previous report [4].

V. Guidelines for Variable–T Noise Modeling

Lastly, we consider a possible use for WBNS. As discussed in Sec. IV-C, RTN, which appears at certain f and T randomly from device to device, is one of the most formidable problems in noise modeling. **Fig. 8** schematically illustrates LF and HF noise baselines. By using WBNS, some temperature ranges in which RTN does not show up can be found. This could enable us to extract baselines for $1/f$ noise and white noise versus T.

There are many proposed $S_{Idn}(f)$ formulas for LF $1/f$ noise [11]. Note that the effect of temperature change on the RTN-free baseline is only to shift $S_{Idn}(f)$ vertically, which nicely gives additional constraints on baseline modeling.

For white noise in the HF region, under the usually satisfied condition of $S_{th} \ll 2qI_d$,

$$S_w(T) = 2qI_d(T) \times F(T) \quad (1)$$

as shown in **Fig. 8**. The use of (1) would be suitable for HF baselines, where F would be a fitting parameter and would play a role of a transfer function between dc and noise properties. A stochastic model for RTN [7] needs to be considered separately on top of it.

VI. Conclusion

We have demonstrated broadband noise characterization of MOSFETs using the noise measurement system at T = 3 K to 300 K and f = 20 kHz to 500 MHz. The wide and fine temperature coverage allowed us to perform WBNS and is effective for noise modeling based on device physics. Although further analyses with data fitting are necessary, we proposed the concept of noise baseline extraction. We believe our approach is beneficial to cryogenic electronics that interface with future large-scale quantum processors.

Acknowledgment

This work was partially supported by NEDO-SBIR.

References

[1] E. Charbon, M. Babaie, A. Vladimirescu, and F. Sebastiano, "Cryogenic CMOS circuits and systems," *IEEE Microwave Mag.*, vol. 22, no. 1, pp. 66–78, Jan. 2021, doi: 10.1109/MMM.2020.3023271.

[2] H. L. Chiang et al., "Design technology co-optimization for cold CMOS benefits in advanced technologies," *IEDM*, pp. 278–281, 2021, doi: 10.1109/IEDM19574.2021.9720573.

[3] K. Ohmori and S. Amakawa, "White noise characterization of n-MOSFETs for physics-based cryogenic device modeling," *Electron Devices Technology and Manufacturing Conference*, 2021, pp. 1–3, doi: 10.1109/EDTM50988.2021.9420837.

[4] K. Ohmori and S. Amakawa, "Variable-temperature noise characterization of N-MOSFETs using an *in-situ* broadband amplifier," *J. Electron Devices Soc.*, vol. 9, pp. 1227–1236, Sep. 2021, doi: 10.1109/JEDS.2021.3112217.

[5] A. Beckers, F. Jazaeri, and C. Enz, "Theoretical limit of low temperature subthreshold swing in field-effect transistors," *IEEE. Electron Device Lett.*, vol. 41, no. 2, pp. 276–279, Feb. 2020, doi: 10.1109/LED.2019.2963379.

[6] P. A. 't Hart, M. Babaie, A. Vladimirescu, and F. Sebastiano, "Characterization and modeling of self-heating in nanometer bulk-CMOS at cryogenic temperatures," *J. Electron Devices Soc.*, vol. 9, pp. 891–901, Oct. 2021, doi: 10.1109/JEDS.2020.2976546.

[7] K. Takeuchi, T. Nagumo, S. Yokogawa, K. Imai, and Y. Hayashi, "Single-charge-based modeling of transistor fluctuations based on statistical measurement of RTN amplitude," *Symp. VLSI Tech.*, pp. 54–55, 2009.

[8] F. J. Scholz and J. W. Roach, "Low-frequency noise as a tool for characterization of near-band impurities in silicon," *Solid-State Electron.*, vol. 35, pp. 447–452, 1992, doi: 10.1016/0038-1101(92)90104-K.

[9] X. Chen, C. H. Chen, and R. Lee, "Fast evaluation of the high-frequency channel noise in nanoscale MOSFETs," *IEEE Trans. Electron Devices*, vol. 65, no. 4, pp. 1502–1509, Apr. 2018, doi: 10.1109/TED.2018.2808184.

[10] K. Ohmori and S. Amakawa, "Direct white noise characterization of short-channel MOSFETs," *IEEE Trans. Electron Devices*, vol. 68, no. 4, pp. 1478–1482, Apr. 2021, doi: 10.1109/TED.2021.3059720.

[11] C. Claeys and E. Simoen, "Low-frequency noise at cryogenic temperatures," in *Low-Temperature Electronics: Physics, Devices, Circuits, and Applications*, San Diego, USA, Academic Press, 2001, ch. 4.3, pp. 430–484.

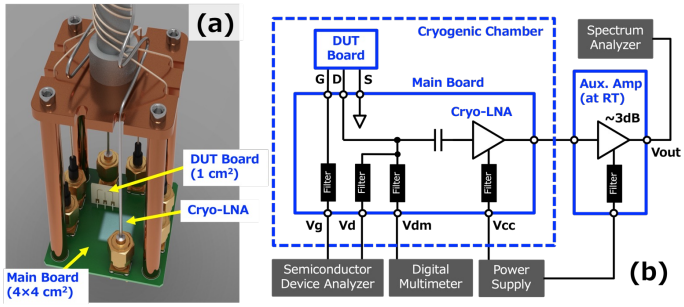

Fig. 1 (a) Broadband cryogenic device noise measurement system. A DUT is mounted by flip-chip bonding on the replaceable DUT board. (b) Schematic diagram of the system. The transmission lines between the DUT and the spectrum analyzer are extensively characterized for calibration.

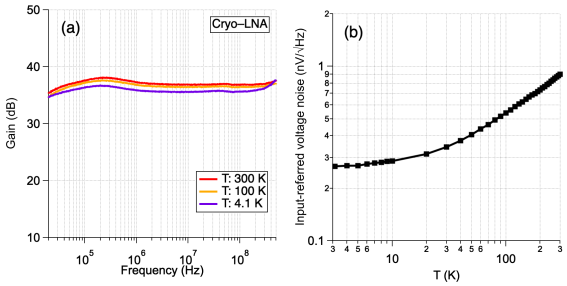

Fig. 2 (a) Gain of the cryo-LNA as a function of f, showing reasonable flatness and thermal stability. (b) Input-referred voltage decreases as temperature decreases down to 30 K and tends to bottom out.

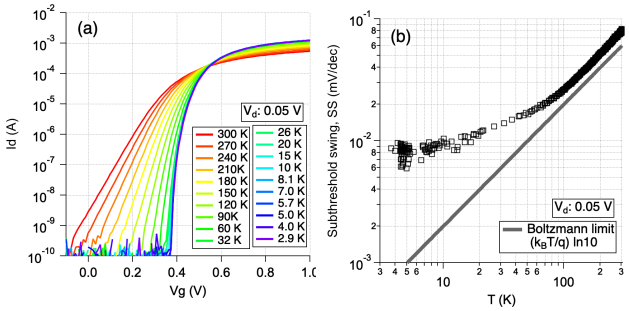

Fig. 3 (a) I_d-V_g curves and (b) subthreshold swing of a MOSFET with L_g=180 nm.

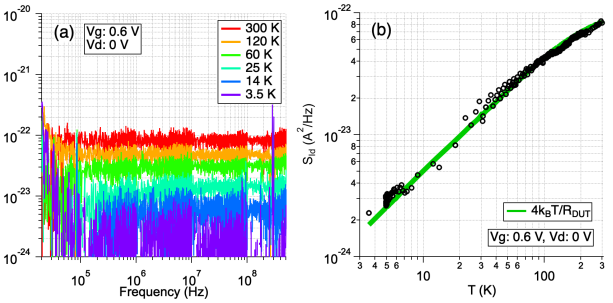

Fig. 4 (a) Temperature dependence of drain current noise spectral density S_{Id} under V_d = 0 V, showing white noise from 20 kHz to 500 MHz. (b) Averaged S_{Id} values in (a) versus temperature. The results are approximately consistent with the theoretical thermal noise of $4k_BT/R_{DUT}$ from 300 to 3 K.

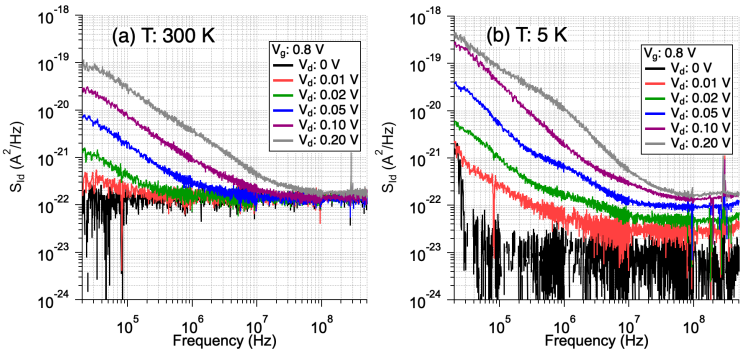

Fig. 5 S_{Id} spectra at (a) T = 300 and (b) 5 K. Transition from 1/f (flicker) noise to white noise is clearly observed. As V_d increases, the level of white noise at T = 300 K increases only slightly, while that at T = 5 K increases substantially. This suggests different main contributors to white noise at 300 K (thermal) and at 5 K (shot).

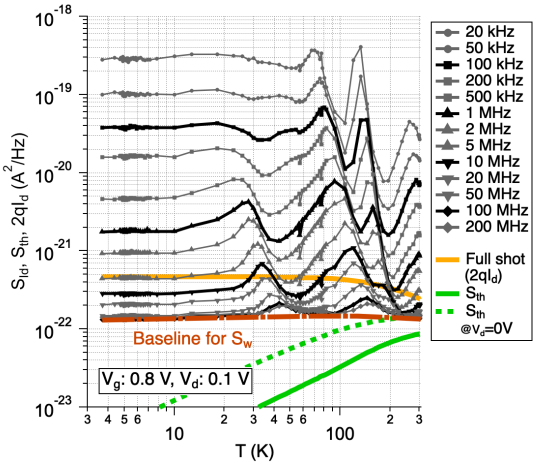

Fig. 6 Noise spectroscopy over extremely wide ranges of T and f, achieved by using the cryogenic noise measurement system for the first time. Examples of the white-noise baselines for f = 200 MHz are drawn together with the thermal noise S_{th} and full-shot noise $2qI_d$.

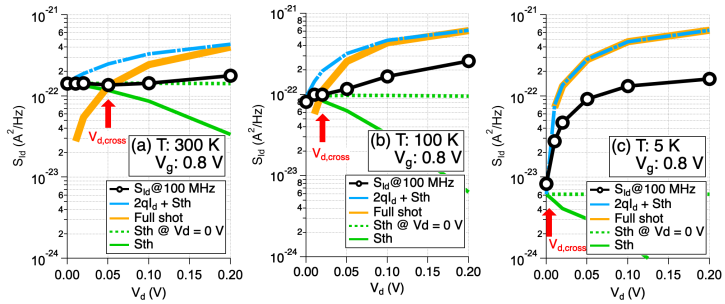

Fig. 7 Measured S_{Id} at 100 MHz, full shot noise ($2qI_d$), and thermal noise (S_{th}) versus V_d. $2qI_d + S_{th}$, shown in blue, gives the upper limit of white noise at 100 MHz if RTN did not exist. As V_d increases, predominant noise changes from thermal to shot noise. The red arrows delineate the border $V_{d,cross}$, at which V_d is ideally equal to $2k_BT/q$. Shot noise dominates at 5 K because $V_{d,cross}$ is very close to 0 V (0.8 mV).

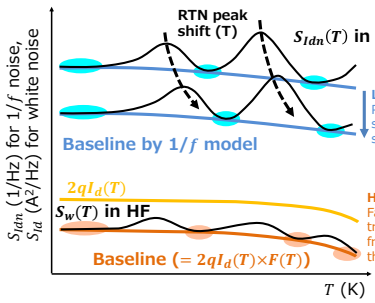

Fig. 8 Extracting RTN-independent device noise models for given bias voltages V_g and V_d. In the low-frequency region, a 1/f noise model is to be applied, while F can be a fitting parameter in the high-frequency region (> 100 MHz). Normalized S_{Idn} is used for 1/f noise analysis. Stochastic RTN that varies from device to device are to be treated separately.